Edinburgh, Scotland
EURONOISE 2009
October 26-28

Reduction of the variable-speed audible magnetic noise radiated by railway traction motors

Jean Le Besnerais[a]
ALSTOM Transport, Petite Forêt, France
Université Lille Nord de France, Ecole Centrale de Lille, L2EP, Villeneuve d'Ascq, France

Vincent Lanfranchi [b]
Université de Technologie de Compiègne, LEC, Compiègne, France

Michel Hecquet [c]
Pascal Brochet [d]
Université Lille Nord de France, Ecole Centrale de Lille, L2EP, France

Andry Randria [e]
ALSTOM Transport, Ornans, France

Sylvain Recorbet [f]
ALSTOM Transport, Semeac, France

Juan Sapena [g]
ALSTOM Transport, Barcelona, Spain

Marc Bekemans[h]
ALSTOM Transport, Charleroi, Belgium

[a] Email address. jean.le_besnerais@centraliens.net
[b] Email address. vincent.lanfranchi@utc.fr
[c] Email address. michel.hecquet@ec-lille.fr
[d] Email address. pascal.brochet@ec-lille.fr
[e] Email address. andry.randria@transport.alstom.com
[f] Email address. sylvain.recorbet@transport.alstom.com
[g] Email address. juan.sapena@transport.alstom.com
[h] Email address. marc.bekemans@transport.alstom.com

ABSTRACT

At low speed, the acoustic power radiated by electrical transport systems can be dominated by a special source of noise called audible magnetic noise. This particular noise comes from magnetic vibrations due to magnetic forces, which are especially strong in traction motors. Some of them are called air-gap Maxwell forces and excite the stator structure, creating harmful resonances during starting or braking. Firstly, this paper presents the phenomenon of magnetic resonances due to Maxwell forces in traction induction motors. Two principal noise sources are analytically identified, namely slotting harmonics and Pulse-Width Modulation (PWM) harmonics. A fully analytical model of the electrical and vibro-acoustic behavior of a traction motor and its PWM supply is then described. This model is validated at different stages (electrical, mechanical and acoustic) using several vibro-acoustic tools (experimental modal analysis, operational modal analysis, operational deflection shapes, spectrograms) and numerical methods (electromagnetic and mechanical finite element method, acoustic boundary element method). On the ground of this model, main magnetic lines are analytically characterized. Finally, this model is coupled with a multi-objective optimization method in order to design a new ALSTOM squirrel-cage induction motor by acting on the rotor geometry and the PWM strategy. The average and maximum magnetic noise levels during starting are minimized, while keeping the same traction characteristics (output torque, efficiency). Two designs are chosen and manufactured. These prototypes are tested and successfully compared to simulations, and a reduction of 15 dB is observed when running the motors in real conditions. It is also shown that the choice of the switching strategy has a 15 dB influence on starting noise.

1. INTRODUCTION

Acoustic noise requirements become stricter in electrical transport systems, especially in light-rail vehicles (LRV) that usually run close from pedestrians and residents. As an example, the European Technical Specification for Interoperability regulates the exterior noise during acceleration. For railway industries, it results in more stringent sound power level (SWL) allocations at train sub-systems levels, and particularly on the traction chain composed of traction motors, converter boxes, and rheostat. These allocations do not only deal with SWL magnitude but also with third octave band spectrum pure tones. Strong tonalities are indeed very unpleasant to hear. Acoustic noise radiated by these components can be classified in three types: “mechanical noise” (e.g. gearbox bearings), “aerodynamic noise” (e.g. converter or motor fans) and “electrical noise” (e.g. inductors, braking resistors, traction motors). The latter source of noise is called “electrical noise”, or audible “magnetic noise”, to be differentiated with high frequency inaudible electromagnetic compatibility noise, as it is caused by magnetic forces acting on parts that are flowed by an electric current. Magnetic vibrations have therefore the characteristic to stop as soon as the vibrating part is current-free. When a LRV starts, traction converters fans usually work at low speed, and braking resistors do not work. Consequently, the major source of noise from traction system is traction motors, which are flowed by high magnitude currents in order to develop the maximal traction torque at starting. Strong magnetic forces can then excite the stator structure during starting, creating harmful resonances as speed varies. It is of prime importance to understand the physical origin of this noise, and be able to realistically simulating it in order to design quiet electrical transport systems.

Two main types of magnetic forces exist: Maxwell forces, and magnetostrictive forces. The latter forces are linked to the intrinsic properties of magnetic materials, and will be neglected in this paper. This particular magnetic force is predominant in electromechanical devices that have no air-gap, such as transformers, which is not the case of traction motors. Moreover, some recent numerical studies have shown that its influence is mainly located in lower frequencies (<1500 Hz), at twice the stator fundamental frequency (which typically varies from 0 to 100 Hz for a two-pole traction motor)[1]. This paper will therefore focus on the audible magnetic noise radiated by traction induction motors due to Maxwell forces.

The first works on the subject started at the early beginning of the twentieth century, where the squirrel-cage induction machines began widespread for their low cost and high robustness. They were of empirical type, and their first concern was to characterize the quietest numbers of slots[2]. It was indeed experienced that depending on the combination of stator winding slots and rotor bars slots numbers, some high-pitch resonances appeared or not. The attempt to analytically characterize and reduce Maxwell forces in the electrical machines started later with Jordan[3] and Alger[4-5] in the 1950's. Their work was mainly pursued by Timar[6-7] in the 1970's. The analytical expressions of Maxwell forces frequencies due to the fundamental current were thus found early, including the harmonic effects of slotting, windings distribution, saturation and eccentricities, and the expression of the number of nodes of slotting force waves was derived at the same time. The characterization of force waves due to PWM was studied later in the 1980's, especially by Timar and Belmans[8-9]. However, the influence of the interaction between slotting and PWM harmonics was only pointed out in 2000's by Lo[10], Okuyama[11] and Hubert[12]. The distinction between rotating and standing vibration waves was first done by Zhu and Howe[13] in an analytical vibro-acoustic model. Verma and Balan[14-16] mainly studied the vibro-acoustic behavior of stators, and also studied the effect of standing versus rotating force waves.
Some of these studies are centered on the exciting forces determination, or on the excited structure characterization; some others do not consider variable-speed effects, or neglect some harmonic sources; finally, the analytical expressions that are established are never validated using deflection shape visualizations, and an accurate comparison between simulation and experiments has never been presented. Following these studies, a fast analytical model of the audible magnetic noise SWL radiated by induction machines has been recently developed by ALSTOM and successfully compared to experiments[17-19]. It includes harmonic effects of saturation[20], slotting[21], and PWM[22-23]. The analytical expressions of Maxwell forces have been extensively characterized with a new formalism[24], leading to innovative low-noise design rules[25]. In this paper, the development of this tool called DIVA is detailed, and it is applied to design two new traction motors with low magnetic noise.

Firstly, the phenomenon of magnetic resonances due to Maxwell forces in traction induction motors is presented, and it is shown that is similar to tyre-road resonances. Two principal noise sources are analytically identified, namely slotting harmonics and Pulse-Width Modulation (PWM) harmonics. In order to be able to predict magnetic noise radiation level, a fully analytical model of a traction motor and its PWM supply is then described. This model is validated at different stages (electrical, mechanical and acoustic) using several vibro-acoustic tools (experimental modal analysis, operational modal analysis, operational deflection shapes, spectrograms) and numerical methods (electromagnetic and mechanical finite element method FEM, acoustic boundary element method BEM). Finally, this model is coupled with a multi-objective optimization method in order to redesign a given squirrel-cage industrial induction motor by acting on the rotor geometry and the PWM strategy. The average and maximum magnetic noise levels are minimized during starting, while keeping the same traction characteristics (output torque, motor efficiency). Two prototypes are designed, manufactured, and tested. Experiments are successfully compared to simulations, and a reduction of 15 dB is observed when running the motors in real conditions. It is also shown that the choice of the switching strategy has a 15 dB influence on noise during starting.

2. MAGNETIC NOISE PHENOMENON

A. Maxwell pressure

The Maxwell force acting on the external radiating part of the motor (stator + frame) can be reduced to a pressure along the air-gap, the thin (~1.5 mm) air space between the stator and the rotor. It can be approximated by

$$P_M = -B_g(t,\alpha)^2 / (2\mu_0) \quad (1)$$

where B_g is the radial air-gap flux density depending on time t and angle α, and μ_0 is the air-gap magnetic permeability. This pressure can be interpreted as the electromagnetic energy per unit volume inside the air-gap. It tends to pull the stator inner surface towards the rotor; this trend in electromechanics is called law of minimal reluctance, as the air-gap reluctance R_g is

$$R_g = g_{eff}(t,\alpha)/\mu_0 \tag{2}$$

where g_{eff} is the mean length of magnetic lines from the rotor to the stator.
A minimal reluctance therefore tends to shorten magnetic lines crossing the air-gap. Both stator and rotor are slotted for stator windings and rotor squirrel-cage bars inclusion (Fig. 1). These slots make the length g_{eff} vary with time and angle.

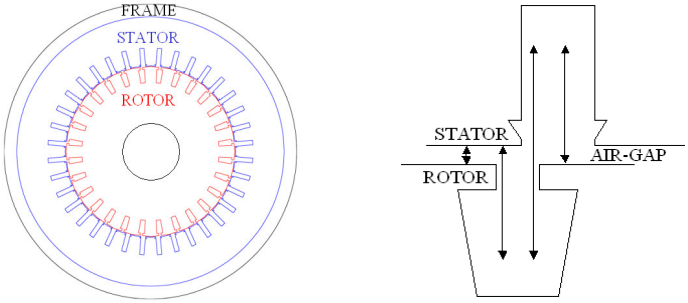

Figure 1: (Left) General overview of the induction machine geometry. (Right) Rotor and stator geometry, and illustration of the four different air-gap reluctance values depending on the relative angular positions of rotor and stator slots. Flux density lines do not necessarily reach the slot bottom.

The following relation links the flux density Bg with the air-gap reluctance:

$$B_g = mmf_T(t,\alpha)/R_g(t,\alpha) \tag{3}$$

where mmf_T is the total air-gap magnetomotive force (mmf). The Maxwell pressure therefore contains reluctance harmonics, also called slotting harmonics, due to g_{eff} variations with time (rotor rotation) and along the air-gap (rotor and stator slotting). Reluctance also changes with saturation level[20] and eccentricities[18], but the magnitude of these harmonics is generally much lower. Total mmf can be decomposed as the sum of stator windings mmf and rotor bars mmf:

$$mmf_T(t,\alpha) = mmf_s(t,\alpha) + mmf_r(t,\alpha) = \sum_{q=1}^{q_s} i_q^s(t) N_q^s(\alpha) + \sum_{b=1}^{Z_{rs}} i_b^r(t) N_b^r(t,\alpha) \tag{4}$$

where $N^{s,r}$ are stator and rotor winding functions, which code stator phase winding and rotor bars spatial distributions, and $i^{s,r}$ are stator and rotor currents.
Stator and rotor currents contain high frequency PWM harmonics. PWM consists in modulating in time the DC input voltage pulses, in order to create through the inductive part of stator windings a current waveform close to a sinusoid at the aimed frequency f_s. This way, the speed of stator field, and therefore the motor speed, can be easily changed. Variable-speed control is necessary for traction applications, but it significantly enrich mmf spectrum with high frequency harmonics.
In conclusion, two main types of harmonics are contained in flux density spectrum, and therefore in Maxwell pressure spectrum: reluctance harmonics due to slotting effects, and PWM harmonics.

B. Resonance phenomena

The Maxwell pressure can be developed in 2D Fourier series as:

$$P_M(t,\alpha) = \sum_{m,\omega} P_{m\omega} \cos(\omega t - m\alpha + \Psi_{m\omega}) \tag{5}$$

It can be seen as the sum of progressive pressure waves of rotation velocity ω/m with $2m$ nodes; some of these pressure waves are precisely due to slotting and PWM. m is also called the spatial order of the pressure wave.

The vibro-acoustic behavior of the stator is close from one of a cylindrical shell (see Fig. 1). Soedel[26] developed the equations describing the interaction between a traveling force wave and a shell. He showed in particular that a resonance occurs if and only if

- the circumferential mode number *n* of the excited shell is the same as the spatial order *m* of the exciting pressure wave
- the frequency of the circumferential mode f_n must be equal to the electrical frequency *f* of the exciting pressure wave. More precisely, this frequency match condition is written as

$$f = \pm f_n \sqrt{1 - 2\xi_n^2} \approx \pm f_n \tag{6}$$

where ξ_n is the modal damping of circumferential mode *n*.

This kind of resonances was first studied in the case of tyre/road resonances[26], as the ground force exciting the rotating tyre can be modeled as a rotating load along a steady tyre.

3. ANALYTICAL MODELING AND VALIDATIONS

A. Maxwell pressure

The analytical model of radial-flux density is based on equations (3-4), where currents are determined using an equivalent circuit whose voltage input comes from a regular sampling triangular PWM model[12]. The obtained flux distribution has been successfully compared to electromagnetic finite element method (FEM) simulations.

B. Dynamic deflections

Static vibrations are first determined by modeling the stator as a ring[7]. For instance, for $m>1$,

$$Y_{mw}^{s} = 12 R_a R_m^{\,3} P_{mw} / (E h^3 (m^2 - 1)^2) \tag{7}$$

where *h* is the thickness of the stator yoke, R_m is the mean stator radius (computed without considering the teeth), *E* is the stator's Young modulus in radial direction and R_a is the stator bore radius. The lowest modes lead therefore to the highest vibrations. Then, dynamic displacements Y^{d}_{mw} are computed using a second order transfer function whose damping factor ξ_m lie between 1% and 4% for traction motors; it is computed using the experimental established by Yang[27]. Natural frequencies are approximated modeling the stator stack as a 2D ring. For $m \geq 2$ they are expressed as[7-14-28]:

$$f_m = f_0 h\, m(m^2 - 1) / (2\sqrt{3} R_m \sqrt{m^2 + 1}) \qquad f_0 = \sqrt{E / (\Delta \rho)} / (2\pi R_m) \tag{9}$$

where f_0 is the zero mode natural frequency, ρ is the stator mass per unit volume, and Δ is the stator mass corrective factor that includes the effect of windings and teeth mass.

Natural frequencies computation was validated using FEM, experimental modal analysis (EMA), and operational modal analysis (OMA)[18] (Fig. 2).

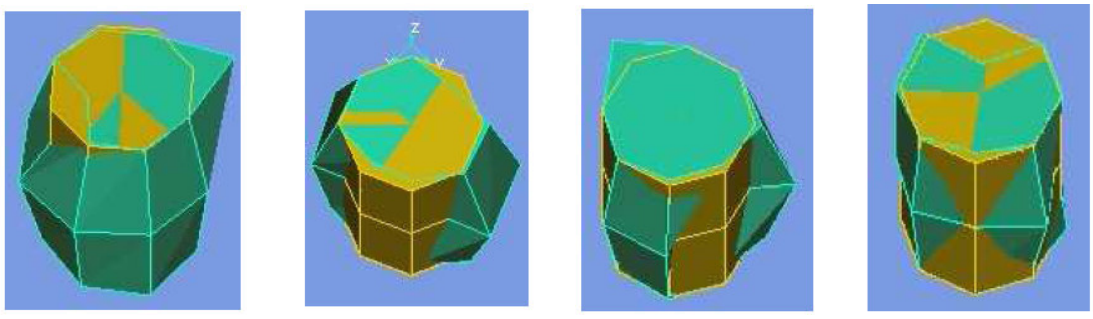

Figure 2: Operational Modal Analysis deflection shapes of circumferential mode 0, 2, 3 and 4.

FEM and EMA validation on the stator considered in this paper are presented in Table 1.

Table 1: *Validation of natural frequencies computation.*

	Analytical computation (Hz)	FEM solid model validation (Hz)	EMA (Hz)
Mode 0	2870	2870	Out of Measurement Range
Mode 2	595	580	606
Mode 3	1535	1570	1402
Mode 4	2885	2840	Out of Measurement Range

C. Vibrations and sound power levels

The vibration waves can then be computed, and the global sound power level (SWL) is obtained by using the radiation factor model of a sphere[6-13]. Some vibratory and acoustic validations have been carried combining a FEM tool and a BEM tool (cf. Fig. 3). Other validations have been made by directly comparing experimental acceleration spectrograms or sonagrams with simulations[18].

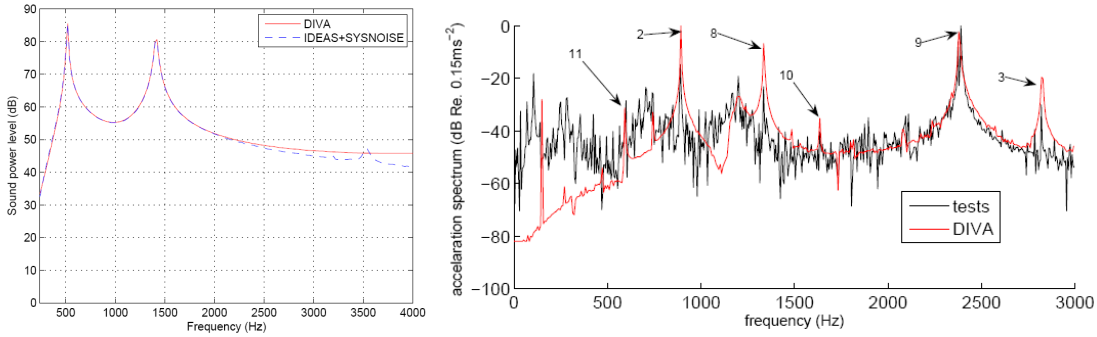

Figure 3: (Left) SWL radiated by a cylindrical shell under a combination of rotating exciting pressure waves of order 2 and 3 computed with analytical model DIVA and with numerical methods (FEM+BEM coupling). (Right) Simulated and experimental vibration spectra at a given motor speed[24].

4. CHARACTERIZATION OF MAGNETIC NOISE AND VALIDATIONS

On the ground of the analytical model, it is possible to analytically derive all the Maxwell pressure harmonics and find the most dangerous ones (low spatial order and high magnitude). This work is extensively presented in reference [18].

A. Slotting harmonics

Their frequencies and spatial orders is presented in Table 2, where $k_{r,s}$ are strictly positive integers, $Z_{r,s}$ are rotor and stator teeth numbers, g is the induction machine slip, and p its pole pair number. The higher these integers are, the lower is the slotting harmonic magnitude. We can see that the slotting harmonics frequencies are proportional to the stator frequency f_s, which is proportional to motor rotational frequency $f_s(1-g)/p$. During starting, all these lines therefore sweep a wide frequency range, increasing the risk of resonances.

Table 2: *Main slotting (left) and PWM (right) magnetic pressure harmonics.*

Slotting pressure harmonics		PWM pressure harmonics	
Frequency f	Spatial order m	Frequency f	Spatial order m
$f_s(k_rZ_r(1-g)/p-2)$	$k_rZ_r-k_sZ_s-2p$	$2f_c-2f_s$	$-2p$
$f_s(k_rZ_r(1-g)/p)$	$k_rZ_r-k_sZ_s$	$2f_c$	0
$f_s(k_rZ_r(1-g)/p+2)$	$k_rZ_r-k_sZ_s+2p$	$2f_c+2f_s$	$2p$

B. PWM harmonics

Main PWM pressure harmonics in case of a regular sampling asynchronous PWM with triangular carrier are reported in Table 2, where f_c is the carrier switching frequency (also called chopping frequency). Note that some similar lines occur around multiples of the switching frequency f_c, $2f_c$, $3f_c$, $4f_c$, etc, but the highest harmonic currents at starting are grouped at twice the switching frequency. Moreover, main PWM harmonics always have 0 or $2p$ spatial orders contrary to slotting harmonics that can have any spatial order.

C. Validations

All these expressions have been validated visualizing some stator operational deflection shapes (ODS). As an example, a slotting vibration at frequency $f_s(Z_r(1-g)/p-2)$ and a PWM vibration at frequency $2f_c$ are illustrated in Figure 4 for a motor with p=2 pole pairs, 27 stator slots and 21 rotor slots[21-22].

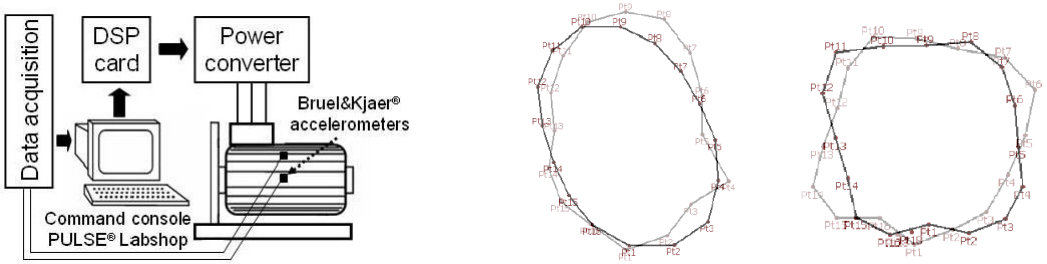

Figure 4: (Left) Experimental setup. (Right) Slotting vibration of order 2=Z_r-Z_s-2p, and PWM vibration of order 4=2p - grey deflections indicate the propagation direction of the vibration wave.

5. APPLICATION AND EXPERIMENTAL RESULTS

In this part, the analytical model is used to design a new prototype based on a 250 kW ALSTOM traction motor with p=2, Z_s=48 and Z_r=38. Its natural frequencies have been characterized in Table 1. To reduce magnetic noise level, while fulfilling the traction characteristics (output torque in function of speed, efficiency, etc), a constrained multi-objective optimization algorithm is used.

A. Optimization algorithm

The optimization algorithm is a multi-objective genetic algorithm, NSGA2[29], which has been modified to handle constraints and mixed variables (i.e. discrete integer variables such as teeth numbers, and continuous variables such as slot dimensions)[31-32]. Only the rotor design is considered, as it less expensive to manufacture. Moreover, acting on the rotor slots number both influence the exciting forces frequencies and spatial orders as seen in Table 2, so larger noise reduction is expected. Three objectives have been considered: maximum noise level and average noise level during starting, and efficiency at nominal speed. These two noise levels are minimized to avoid a traction motor that would have a small average noise level, but a single high resonance, as well as a traction motor that would have no particular resonance, but a high average noise level[30]. Two designs have been selected in the final Pareto front: one with 36 rotor slots, and the other one with 60 slots. Note that these two numbers are symmetrical with respect to stator slots number (36=48-12 and 60=48+12).

B. Simulation results

Simulation results showed that the prototypes significantly improved average and maximum noise levels. Noise reduction was expected to reach 20 dB on the 36 rotor slots, because a resonance due to saturation on the initial motor with 38 rotor slots was avoided (Fig. 5)[20].

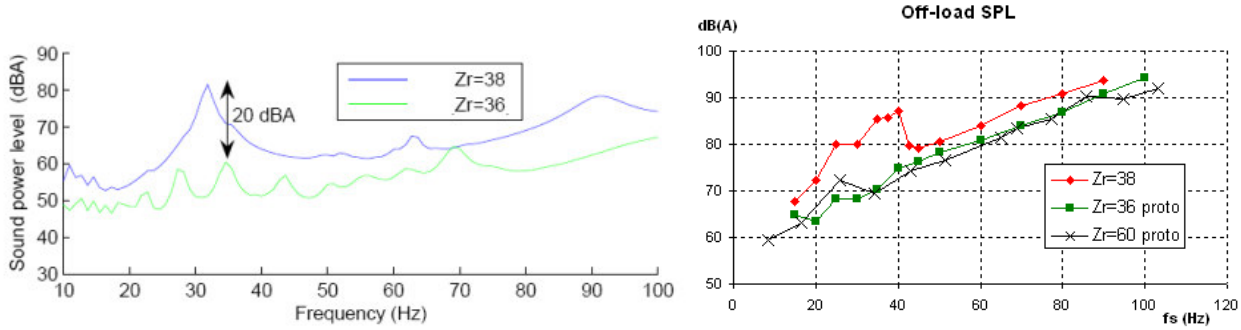

Figure 5: (Left) Expected magnetic noise reduction in function of stator frequency with DIVA for the first prototype. (Right) Experimental SWL radiated by the initial motor and the two prototypes in off-load case.

C. Experimental results

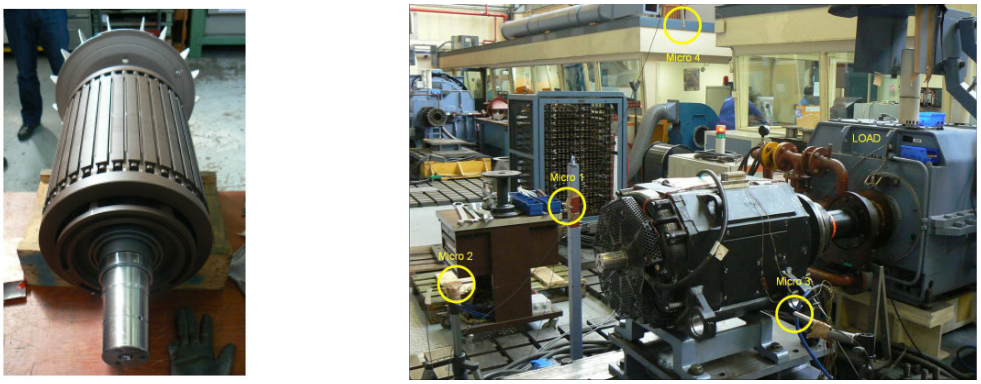

Figure 6: (Left) Rotor prototype with Z_r=36 slots. (Right) Experimental set-up.

The two prototypes have been manufactured and tested (Fig. 6). In off-load case (without any resistive effort on the rotor shaft), as predicted by simulations, up to 15 dB reduction was observed as starting (Fig. 5). No significant resonance due to slotting or saturation occurred, and the sound-pressure (SPL) linearly increases with speed due to aerodynamic noise, as the motor is opened self-ventilated. The magnetic noise source has been efficiently cancelled.

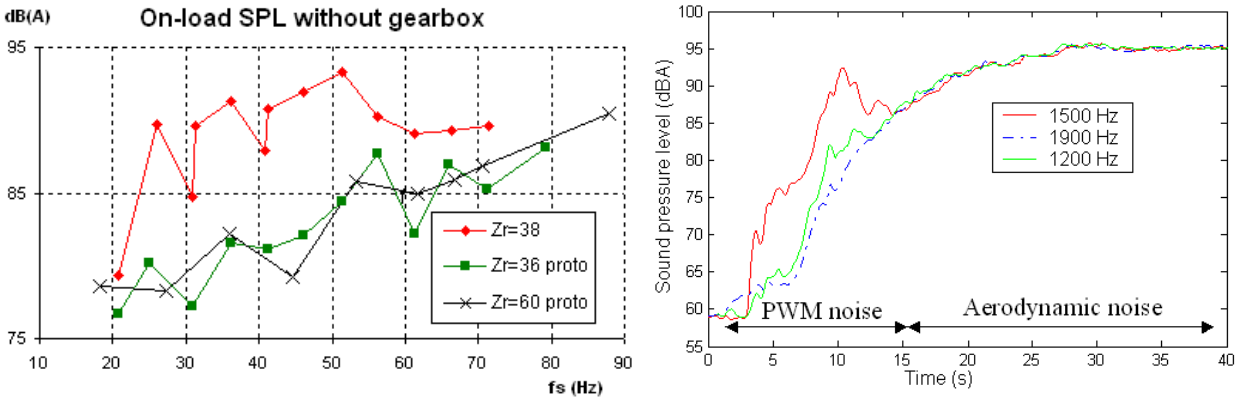

Figure 7: (Left) Experimental SPL radiated at 1m by initial motor and prototypes in on-load case. (Right) Experimental SPL measured during Zr=60 runup with different PWM asynchronous frequencies.

Noise reduction is still present in on-load case, as shown in Fig. 7 where the gearbox lines have been cancelled by postprocessing spectra in order to only compare aerodynamic + magnetic noise levels. The effect of PWM strategy on noise has also been studied. As predicted by analytical computations, the maximum SPL is obtained when the PWM vibrations near twice the switching frequency enter in resonance with 0 and 2*p* stator modes near 3000 Hz, that is to say for f_c=1500 Hz. Reducing PWM noise is particularly important as it is a source of roughness[33] at starting, when main PWM lines have close frequencies (cf. Table 2). In Fig. 7 the SPL becomes independent of f_c over 30 km/h (>15s) as it is dominated by fan noise. f_c>1900 Hz makes PWM noise negligible even at low speed but it increases inverter losses and heating. The switching frequency influence can therefore have a 15 dB impact during starting. Fig. 8 shows one of the prototypes sonogram from f_s=0 to 100 Hz: one can distinguish mechanical and aerodynamic lines (1), main PWM lines (2) around twice the switching frequency, and slotting lines (3) that have been drastically reduced by a proper choice of slot rotor numbers and opening width.

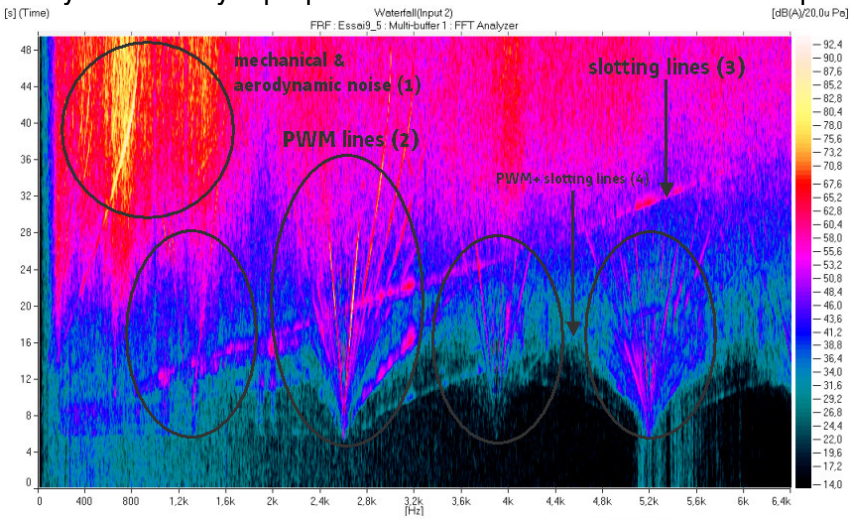

Figure 8: Experimental SPL sonogram of Z_r=36 prototype in asynchronous PWM case (f_c=1280 Hz).

6. CONCLUSIONS

A fully analytical model of ALSTOM PWM-fed traction induction machines has been elaborated in order to compute traction characteristics and audible magnetic noise level due to Maxwell pressure. With the help of an optimization algorithm, two new prototypes have been defined. Expected noise reduction with simulation has been experimentally validated: noise level has been reduced of 10 dB at starting in on-load case. The optimization of the PWM asynchronous frequency from 1280 Hz to 1000 Hz has led to an additional 5 dB reduction at the same speed, so a total noise reduction of 15 dB has been reached during motor starting in real conditions.

ACKNOWLEDGMENTS

This work has been partly funded by the French ADEME.

REFERENCES

1. A. Belahcen, Magnetoelasticity, magnetic forces and magnetostriction in electrical machines, ¨hD thesis, Helsinki University of Technology, Finland, 2004.
2. G. Kron, “Induction motor slot combinations: rules to predetermine crawling vibration, noise and hooks in the speed-torque curve”, in *AIEE Transactions* **50***,* 1931
3. H. Jordan, Electric motor silencer - formation and elimination of the noises in the electric motors, W. Giradet-Essen Editor, 1950.
4. Alger, “The acoustic behavior of induction motors”, in *JASA* **25**(4), 1953.
5. P.L. Alger, The nature of polyphase induction machines, John Wiley & Sons, Inc., 1951.
6. P.L. Timar and J.C.S. Lai, “Acoustic noise of electromagnetic origin in an ideal frequency-converter-driven induction motor”, in *IEE Proc. on Electr. Power Appl.* **141**, n°6, pp.341-346, 1994.

7. P.L. Timar, Noise and vibration of electrical machines, Elsever, London 1989.
8. R. Belmans, L. D'hondt, A.J. Vandenput and W. Geysen, “Analysis of the audible noise of three-phase squirrel-cage induction motors supplied by inverters”, in *IEEE Trans. on Ind. Appl.* **23**, 1987.
9. R. Belmans, D. Verdyck, W. Geysen and R. Findley, “Electro-mechanical analysis of the audible noise of an inverter-fed squirrel cage induction motor”, in *IEEE Trans. on Ind. Appl.* **27**(3), 1991.
10. Y. Okuyama and S. Moriyasu, “Electromagnetic noise of induction motors driven by PWM inverters,” in *Electrical Engineering in Japan*, **133**(3), 2000.
11. W.C. Lo, C.C. Chan, Z.Q. Zhu, L. Xu, D. Howe and K.T. Chau, “Acoustic noise radiated by PWM-controlled induction machine drives”, in *IEEE Trans. on Ind. Elec.* **47**(4), pp.880-889, 2000.
12. A. Hubert, Contribution à l’étude des bruits acoustiques générés lors de l’association machines électriques - convertisseurs statiques de puissance. Application à la machine asynchrone, Ph.D. dissertation, Université des Technologies de Compiègne, France, 2000 (in French).
13. Z.Q. Zhu and D. Howe, “Improved methods for prediction of electromagnetic noise radiated by electrical machines”, in *IEE Proc. on Electr. Power Appl.* **141** (2), pp.109-120, 1994.
14. S.P. Verma and R.S. Girgis, “Method for accurate determination of resonant frequencies and vibration behaviour of stators of electrical machines”, in *IEE Proc. on xxx.* **128**(1), 1981.
15. S.P. Verma and A. Balan, “Experimental investigations on the stators of electrical machines in relation to vibration and noise problems”, in *IEE Proc. on Elec. Power Appl.* **145**(5), 1981.
16. S.P. Verma and A. Balan, “Determination of radial-forces in relation to noise and vibration problems of squirrel-cage induction motors”, in *IEE Proc. on En. Conversion.* **9**(2), 1994.
17. A. Ait-Hammouda, Prédimensionnement et étude de sensibilité vibro-acoustique de machines à courant alternatif et à vitesse variable, Ph.D. dissertation, USTL, Lille, France, 2005 (in French).
18. J. Le Besnerais, Reduction of magnetic noise in PWM-supplied induction machines – low-noise design rules and multi-objective optimisation, PhD Thesis, Ecole Centrale de Lille, 2008.
19. J. Le Besnerais, V. Lanfranchi, M. Hecquet, P. Brochet, S. Récorbet, J. Sapena and A. Randria, “Characterization of the audible noise emitted by traction motors in railway rolling stock,” in *Proceedings of the Internoise Conference*, Shanghai, 2008.
20. J. Le Besnerais, V. Lanfranchi, M. Hecquet, G. Lemaire, E. Augis and P. Brochet, “Characterization and reduction of magnetic noise due to saturation in induction machines,” in *IEEE Trans. on Magnetics* **45**(4), 2009.
21. J. Le Besnerais, V. Lanfranchi, M. Hecquet, and P. Brochet, “Optimal slot numbers for magnetic noise reduction in induction machines,” in *IEEE Trans. on Mag*, 2009.
22. J. Le Besnerais, V. Lanfranchi, M. Hecquet, P. Brochet, and G. Friedrich, “Characterisation of the radial vibration force and vibration behaviour of a pulse-width modulation-fed fractional-slot induction machine,” in *IET Electric Power Applications* **3**(3), 2009.
23. J. Le Besnerais, V. Lanfranchi, M. Hecquet, P. Brochet, and G. Friedrich, “Characterization and reduction of magnetic noise due to PWM in induction machines,” in *IEEE Trans. on Industrial Electronics*, 2009.
24. J. Le Besnerais, V. Lanfranchi, M. Hecquet, P. Brochet, and G. Friedrich, “Acoustic noise of electromagnetic origin in a fractional-slot induction machine,” in *COMPEL*, **27**(5), 2008.
25. J. Le Besnerais, V. Lanfranchi, M. Hecquet and P. Brochet, “Optimal choice of slot openings for magnetic noise reduction,” in *IEEE Trans. on En. Conv,* 2009.
26. W. Soedel, Vibrations of shells and plates, Marcel Dekker, 1993.
27. S.J. Yang, Low noise electrical motors, Clarendon Press, Oxford, 1981.
28. J.F. Gieras, C. Wang and J.C. Lai, Noise of polyphase electric motors, CRC Press, 2005.
29. K. Deb, A. Pratap, S. Agarwal and T. Meyarivan, “A fast and elitist multiobjective genetic algorithm: NSGA-II”, in *IEEE Trans. on Ev. Comp.*, **6**(2), 2002.
30. J. Le Besnerais, V. Lanfranchi, M. Hecquet, and P. Brochet, “Multiobjective optimization of the induction machine with minimization of audible electromagnetic noise,” in *EPJ-AP* **39**(2), 2007.
31. J. Le Besnerais, V. Lanfranchi, M. Hecquet, and P. Brochet, “Multi-objective optimization of induction machines including mixed variables and noise minimization,” in *IEEE Trans. on Mag.*, **44**(6), 2008.
32. J. Le Besnerais, A. Fasquelle, V. Lanfranchi, M. Hecquet, and P. Brochet, “Mixed-variable optimal design of induction motors including efficiency, noise and thermal criteria,” in *Proceedings of the International Conference on Engineering and Optimization*, 2008.
33. E. Zwicker and H. Fastl, Psychoacoustics, Facts and Models, Springer-Verlag, Berlin Heidelberg, Germany, 1992.